EUROPEAN ORGANIZATION FOR NUCLEAR RESEARCH

CERN/PS/87-60 (PO)
31 July 1987

THE d.c. POWER SUPPLIES (3000 A, 40 V) OF THE SEPTUM MAGNETS FOR PARTICLE INJECTION INTO THE ELECTRON AND POSITRON ACCUMULATOR

M. Métais, G. Simonet, and F. Voelker

ABSTRACT

The operational requirements and the main features of the septum power supplies are briefly mentioned.

The power circuit layout, chosen for reasons of simplicity, overall efficiency, and reliability, is described. It includes two double transformers, four three-pulse thyristor rectifiers paralleled through the chokes of the passive smoothing filter, an active ripple filter, and a mechanical off-load polarity changer.

The design criteria of the regulation circuit and the problems raised by the insertion of the active filter in the current loop are presented.

Some more specialized design aspects are treated in the Appendices.

CONTENTS

List of figures

List of Tables

1. INTRODUCTION

The pre-injector of LEP [1,2] consists of a 200 MeV linac for positron production, followed by a 600 MeV linac for particle acceleration, and of the electron/positron accumulator (EPA) ring.

The linacs deliver short particle pulses at a repetition frequency of 100 Hz to EPA, whose role is to build up and store the required eight intense bunches at 600 MeV before their transfer to the PS.

The geometry of the machines is such that the 600 MeV linac intersects the race-track shaped EPA ring and that injection of particles occurs at opposite points inside the ring. The short beam lines between the linac and the injection point impose a deflection angle of ~ 30 ° on the d.c. septum magnets.

The electron and positron bunches are finally ejected from the EPA into the beam transfer lines to the PS by a common pulsed extraction septum.

2. LOAD CHARACTERISTICS

Two pairs of d.c. magnets [3] (called HIE-SMH 33 and HIP-SMH 33), each pair consisting of a 12-turn thick septum magnet and of a 4-turn thin septum magnet, optimized for the particular injection geometry and beam parameters, are located internally on opposite sides of the EPA ring and deflect the incoming e^-e^+ particles into the injection orbit of the machine.

The two septum magnets of each pair are electrically connected in series and cooled by a dedicated closed circuit, low-oxygen content, high-pressure demineralized water system having an inlet water temperature of 22.5 °C.

The magnet cores are made from standard 1.5 mm silicon grade steel laminations, while the winding conductor consists of OFHC copper tube with 6 mm x 6 mm outside dimensions and a 2 mm x 2 mm cooling hole.

The basic magnet parameters are given in Table 1.

Table 1

Parameters of the injection septum magnets

	4-turn magnet	12-turn magnet	Magnet pair
Bending angle (degree)	7.25	21.75	29
Nominal magnetic induction (T)	0.52	1.55	
Laminated core length (mm)	500	500	
Vertical/horizontal aperture between poles (mm)	25/91	25/91	
Nominal current (A)	2720	2720	
Septum current density (A/mm^2)	85	85	
Power dissipation (kW)	19.7	66.8	86.5
Cooling water flow (l/min)	18.3	60	
Septum thickness (mm)	6	18	
Coil resistance (mΩ)	2.68	9.18	11.86
Magnet inductance at 1 kHz (μH)	35	300	335

3. PERFORMANCE REQUIREMENTS

The main performance specifications and design parameters of the power supplies are given in Table 2.

The basic layout of the power supply is shown in Fig. 1.

The two power supplies are located in an equipment building at 20 and 40 m distance from the EPA injection points and are connected to the two pairs of septum magnets via 8 and 16 parallel 240 mm^2 copper cables.

The requested current stability has been achieved by adding to the basic power circuit an active ripple filter, which works independently and can be switched in and out during operation.

Table 2

Specified power supply design parameters

Input voltage	380 V, 50 Hz, 3 phase
Nominal/Maximum ouput current	2750/3000 A
Output voltage/power at 3000 A	$\leq$ 40 V/120 kW
Current control range	30 - 3000 A
Current stability and ripple at nominal current	$\pm$0.01%
Total nominal load impedance	13 mΩ, 365 µH
Off-load mechanical polarity changer	yes
Overall power conversion efficiency	$\geq$ 0.85
Ambient air temperature	$\leq$ 40 °C
Cooling water temperature	$\leq$ 30 °C

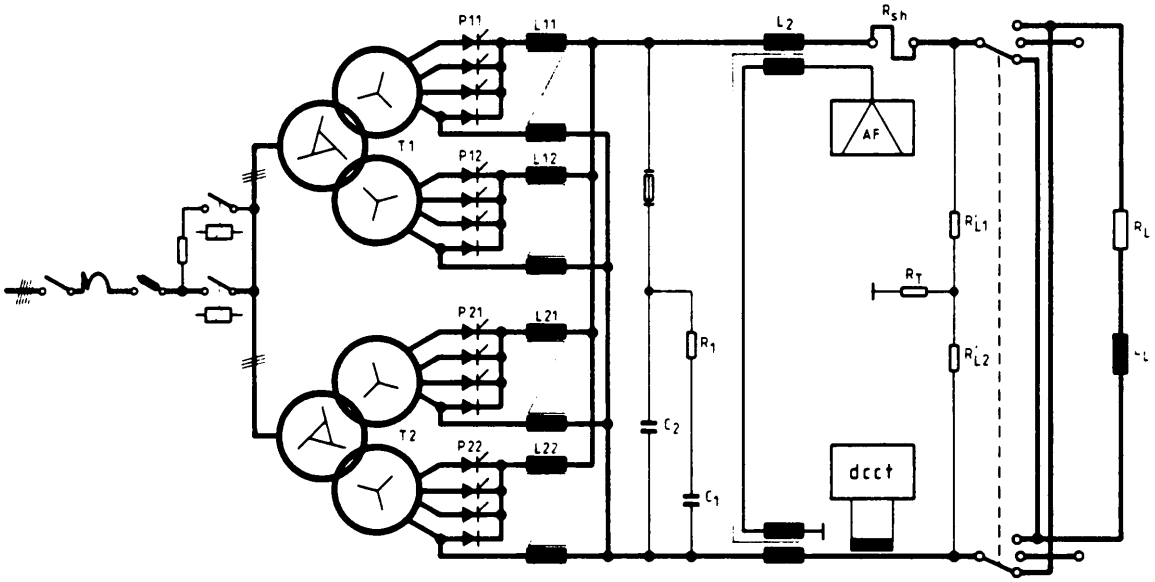

Fig. 1 Schematic layout of power supply

The development of such a system opens up the interesting possibility of replacing the lossy series transistor regulators of the existing high-current d.c. power supply in order to obtain substantial energy saving.

Photographs of the power supply and its internal layout are shown in Fig. 2.

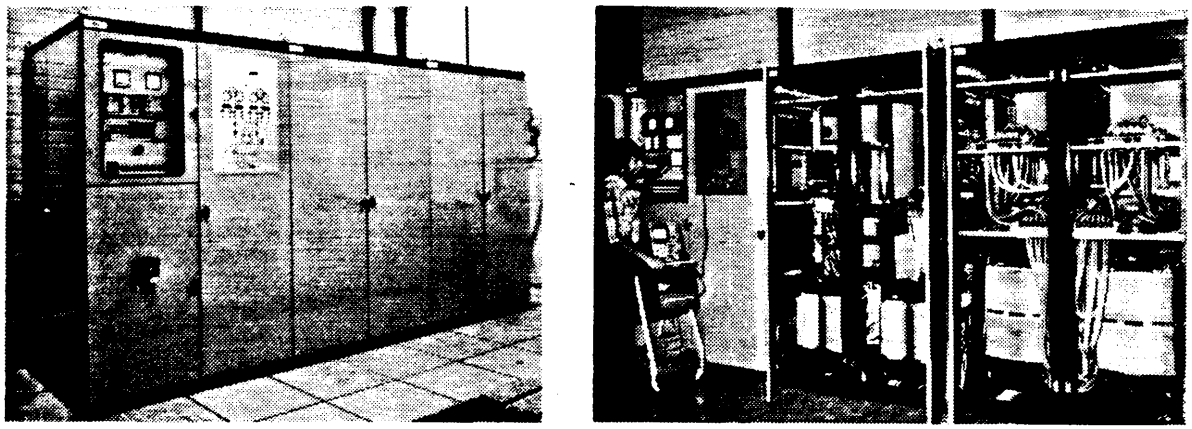

Fig. 2 Front view of the power supply and its internal layout

4. DESIGN CRITERIA AND LAYOUT

4.1 Power section

As shown in Fig 1, the power part mainly consists of the transformer inrush current limiting circuit, of two double 3-phase transformers, of four 3-way thyristor rectifiers with free-wheeling diode, of the passive smoothing filter, of the active ripple filter, and finally of the electro-mechanical polarity changer.

4.1.1 *Inrush current limitation*

An auxiliary 22 Ω resistor is switched in series with the power transformers to allow surge-free premagnetization and is eventually short-circuited by the main contactor.

The design of the inrush current limiting circuit is treated in Appendix A.

4.1.2 *Power transformers*

As schematically shown in Fig. 3, the two identical four-winding rectifier transformers have extended delta primaries and star with neutral secondaries. The two sets of primary and secondary windings are located on the upper and the lower part of each column of the magnetic circuit. The secondary windings are located internally close to the core.

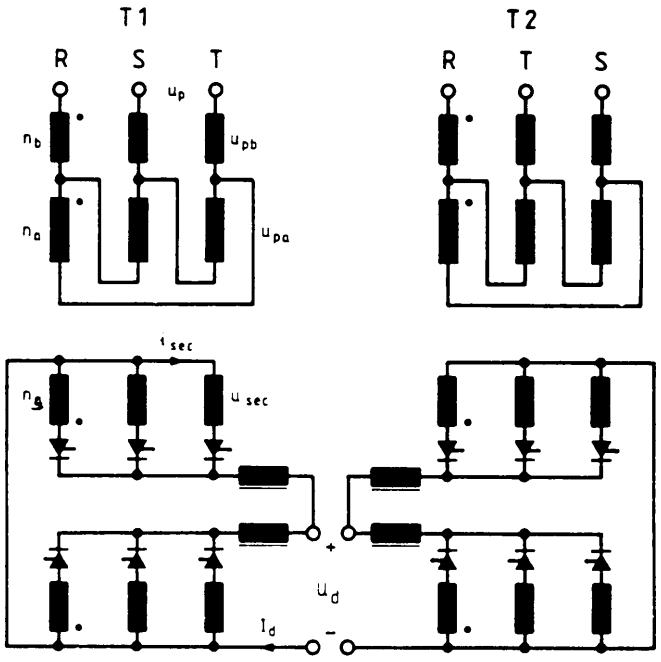

Fig. 3 Power transformer layout

The transformers are of the dry type; their main parameters are given in Table 3. The required ±15° phase displacement of the secondary voltage vectors of the two power transformers is obtained by changing the a.c. phase connection sequence on the primary.

In view of the fact that the extended delta-star transformer is used now very frequently in magnet power supplies, as it has some advantages with respect to the polygon-star connection, it is treated more generally in Appendix B.

Table 3

Parameters of the power transformers

Maximum/nominal primary voltage	(V)	418/380
Design power ratings	(kVA)	95
Short-circuit voltage: U_k	(%)	5
Magnetizing current	(%)	4
Isolating materials/operating temperature class		H/E
Type of core lamination		M6T35
Iron cross-section	(cm^2)	145.5
Number of turns: primary (n_a)		45 (two layers of 23 and 22 turns)
(n_b)		26
secondary (n_s)		10 (three layers of 3, 3, and 4 turns)
Winding currents I_a-I_b-I_s	(A)	72-125-443
Winding resistance at 25 °C R_a-R_b-R_s	(mΩ)	24-11-0.48
Losses: P_J	(W)	2000
P_0 at 380 V	(W)	450
Number of cooling channels		6
Dimensions: W x D x H	(mm^3)	660 x 460 x 880
Weight	(kg)	630
Manufacturer		TRAFOMEC/I

4.1.3 *Thyristor rectifiers*

Four 3-way thyristor rectifiers with freewheeling diodes are fed by the star secondaries of the two power transformers, and their d.c. terminals are connected in parallel through the two-winding chokes of the passive filter, which therefore replace the more common interphase reactors.

This circuit produces a d.c. voltage with a 12-pulse basic ripple and is particularly suitable for high-current power supplies owing to the lower losses in the thyristors and the absence of interphase reactors.

The rectifier semiconductors are SEMIKRON SKT 340/12 and SKN 501/08 flat-pack types; they are clamped between short copper bars force-cooled by demineralized water.

The cooling circuit is designed for a $\Delta\theta$ of 4 °C per rectifier with a water flow of 5 l/min; consequently, the four rectifiers can easily be cooled in series. RC and transorb protecting elements are connected across the thyristors. A thermocontact controls the maximum temperature of the rectifier assembly.

The very compact rectifier is shown in Fig. 4.

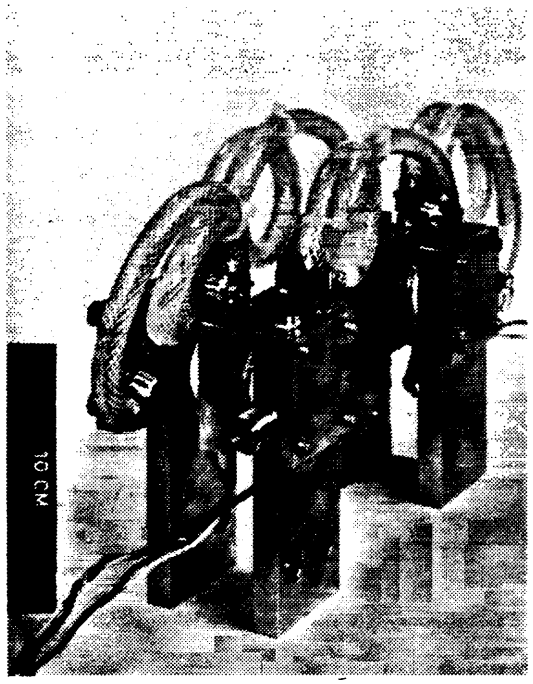

Fig. 4
Water cooled 3-way rectifier assembly with free-wheeling diode

Much care has been taken concerning the power cabling between transformer secondaries, rectifiers, and filter chokes so as to equalize, as far as possible, the parallel connected line impedances of the circuit.

The output voltage waveform of the four rectifiers for a d.c. current of 1000 and 2700 A is shown in Fig. 5 together with a secondary-phase voltage waveform of the transformer.

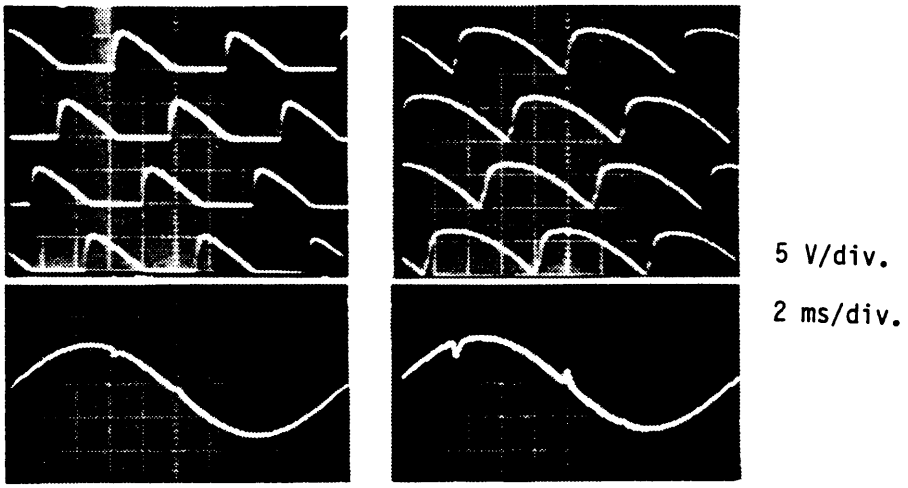

Fig. 5 Output voltage and a.c. voltage waveforms of the four rectifiers

4.1.4 *Passive filter*

The main parameters of the passive LCR smoothing filter are given in Table 4, where

$$\frac{C_1}{C_2} = n = 4 \ ,$$

$$\frac{1}{\omega_0} = \tau_0 = \sqrt{L_1 (C_1 + C_2)} \ ,$$

$$\xi = \frac{R_1}{2} \sqrt{\frac{(C_1 + C_2)}{L_1}} \ .$$

Table 4

Parameters of the LCR filter

L_1 (mH)	R_1 (Ω)	C_1 (mF)	C_2 (mF)	ξ	$\frac{\omega_0}{2\pi}$ (Hz)	$\frac{\omega_1}{2\pi}$ (Hz)	$\frac{\omega_2}{2\pi}$ (Hz)	$\frac{\omega_3}{2\pi}$ (Hz)	χ
$\frac{0.8}{4}$	0.15	60	15	1.45	41.1	17.7	21.3	83.75	0.4

The no-load transfer function is given by the relationship

$$\frac{U_r}{U_R} = \frac{1 + 2\xi[n/(n+1)]\tau_0 s}{\tau_0^2 s^2 \{1+[2n/(n+1)^2]\xi\tau_0 s\} + [2n/(n+1)]\xi\tau_0 s+1}$$

$$= \frac{[1+(s/\omega_1)]}{[1+(s/\omega_2)]\ [1+2X(s/\omega_3) + (s^2/\omega_3^2)]} \ .$$

The frequency and step response of the LCR filter under no-load and nominal (magnet)-load conditions are shown in Fig. 6.

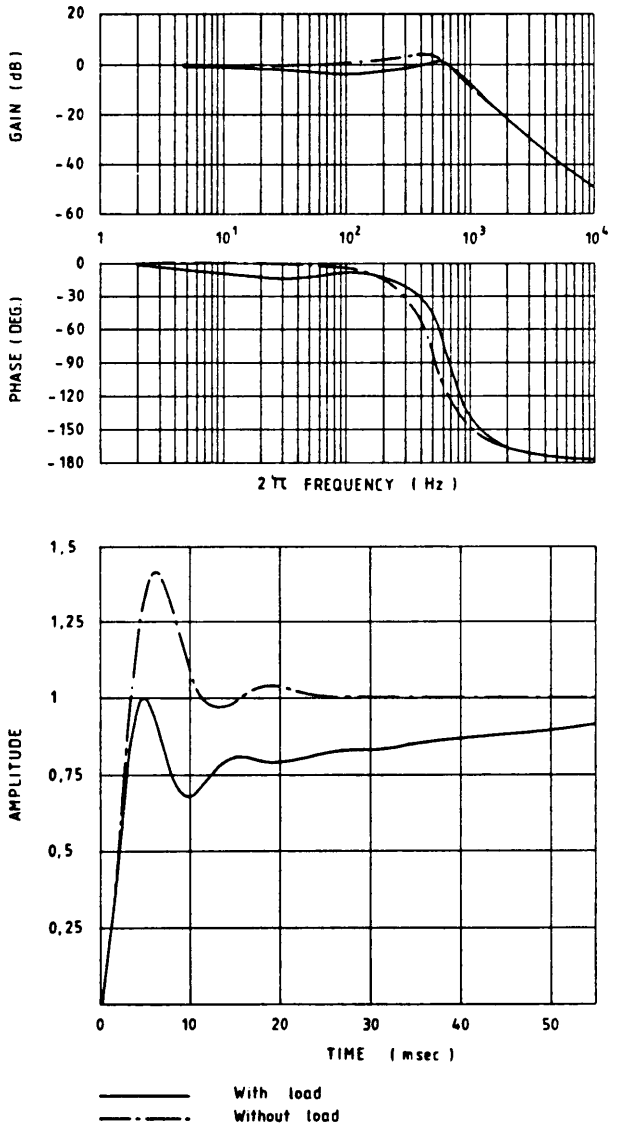

Fig. 6 Frequency and step response of passive LCR filter

The characteristics of the passive filter components, consisting of four chokes and two polarized capacitor banks with a damping resistor are given in Table 5.

Table 5

Characteristics of the passive filter components

Chokes		L_{11}, L_{12}, L_{21}, L_{22}	
Inductance at 750 A	(mH)	0.8	
Power rating	(kVA)	50	
Temperature class		H/E	
Lamination		M6T35	
Iron corrector	(cm^2)	182	
Conductor Al	(mm^2)	945	
Number of turns		2 x 14	
Geometric air gap	(mm)	2 x 11.4	
Effective air gap	(mm)	2 x 10.2	
Resistance at 25 °C	(mΩ)	2 x 0.375	
Dimensions (W x D x H)	(mm^3)	480 x 360 x 620	
Weight	(kg)	300	
Capacitors (Type PEH169 RIFA)		C_1	C_2
Capacitance	(mF)	4 x 15	10 x 1.5
Voltage	(V)	63	250
Current at 85 °C and 100 Hz	(A)	13.9	5.5
Resistor		R_1	
Resistance	(Ω)	0.15	
Power	(W)	200	

4.1.5 *Polarity-reversal device*

The power supply is fitted with a mechanical polarity-reversal device of the MULTICONTACT crossbar type. It allows off-load manual selection of the output polarity, or the

connection of a dummy load to the output, by inserting plugs in two of six interlocked crossbar positions.

4.2 Active Ripple Filter

The active ripple filter has been specifically designed for the present high-current d.c. power supplies with a low-impedance septum magnet as load, for which an attenuation of 15 to 20 dB of the output voltage ripple can be achieved.

Its power stage, a hybrid industrial component is coupled to the power supply output via a choke with two windings.

The characteristics of the power amplifier and of the coupling choke are given in Table 6.

The active filter drive circuit and power amplifiers are shown in Fig. 7.

The analysis and design of the active filter are treated in Appendix D.

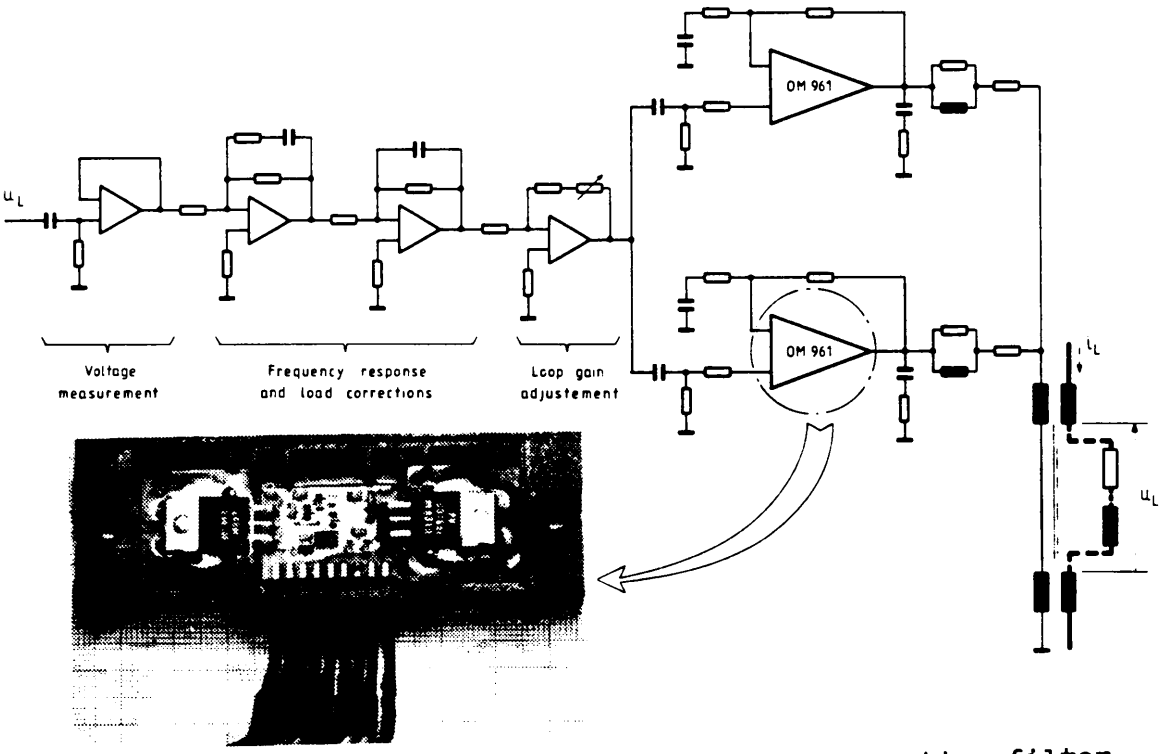

Fig. 7 Drive circuit and power amplifiers for active filter

Table 6

Active filter choke and amplifier characteristics

Coupling choke			
Secondary inductance at 3000 A		(mH)	0.05
Primary/secondary resistance at 25 °C		(mΩ)	200/0.1
Number of turns n_1/n_2			138/8
Power ratings		(kVA)	50
Temperature class			H/E
Iron cross-section		(cm^2)	144
Winding cross-section	Cu	(mm^2)	35
	Al	(mm^2)	2000
Lamination			M6T15
Dimensions: W x D x H		(mm^2)	460 x 370 x 760
Weight		(kg)	280
Power amplifier (Philips OM961)			
Supply voltage		(V)	±35
Sinus output power		(W)	60
Nominal load impedance		(Ω)	8
Power bandwidth		(Hz)	20-40000
Input impedance		(kΩ)	10
Output impedance		(Ω)	0.05
Open-loop gain		(dB)	80
R_{th} of heat sink		(K/W)	0.8
Units in parallel via 1 Ω			2

4.3 Regulation

The regulation, which is schematically represented in Fig. 8, is a multiloop system conceived to obtain the specified magnet current stability and precision by adapting the functional blocks to the characteristics of the load, the power circuit, and the thyristor gate control under given ambient and

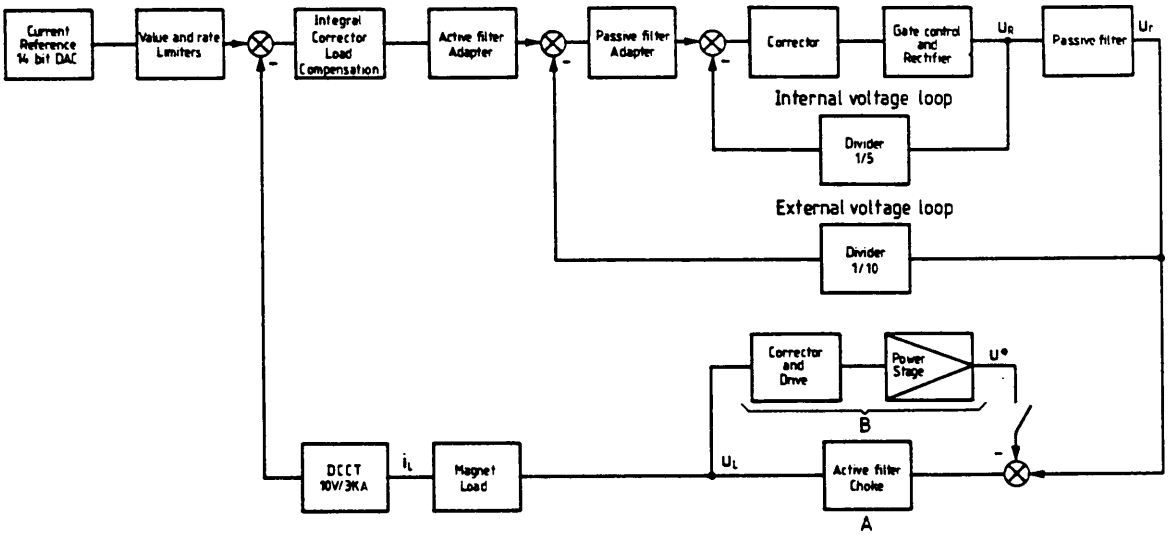

Fig. 8 Schematic diagram of voltage and current regulation

mains conditions. It has been designed making use of a specialized (Linear System Analysis) computer program and optimized by measuring the frequency response of the building blocks.

4.3.1 *Voltage-control loops*

The design concept of the regulation implies that the voltage-control loops cope with the lower frequency ripple and transients, therefore releasing the active filter, and that the latter acts as an independent second filtering stage for the typical rectifier ripple harmonics (see Appendix C).

The internal fast voltage-control loop, sometimes part of a modern thyristor gate control set, gives a symmetric rectified voltage and reacts to any mains voltage perturbation and transient.

The external loop further reduces undesired lower frequency voltage variations, compensates the second-order passive filter frequency response, and adapts the closed-loop voltage-control transfer function to the external current loop.

For practical reasons of circuit-board standardization, a gate-control set with a transfer function having a 45° phase-lag frequency of the order of 70 Hz, despite the 12-pulse rectifier, has been used. Consequently, the trade-off between operation of

the active filter and of the voltage-control loops could not be fully optimized.

In fact, a gate-control set with a 300 Hz flat gain characteristic has also been tested in the course of this development and a further improvement of a factor of two in output current ripple has been obtained with the present active filter.

4.3.2 *Active-filter control loop*

The active filter drive and power stage is included in the feedback (B) path of the loop; it can be switched-in or -out during operation without disturbing the current-control loop. This feature has been of great help during testing and setting -up of the power supply.

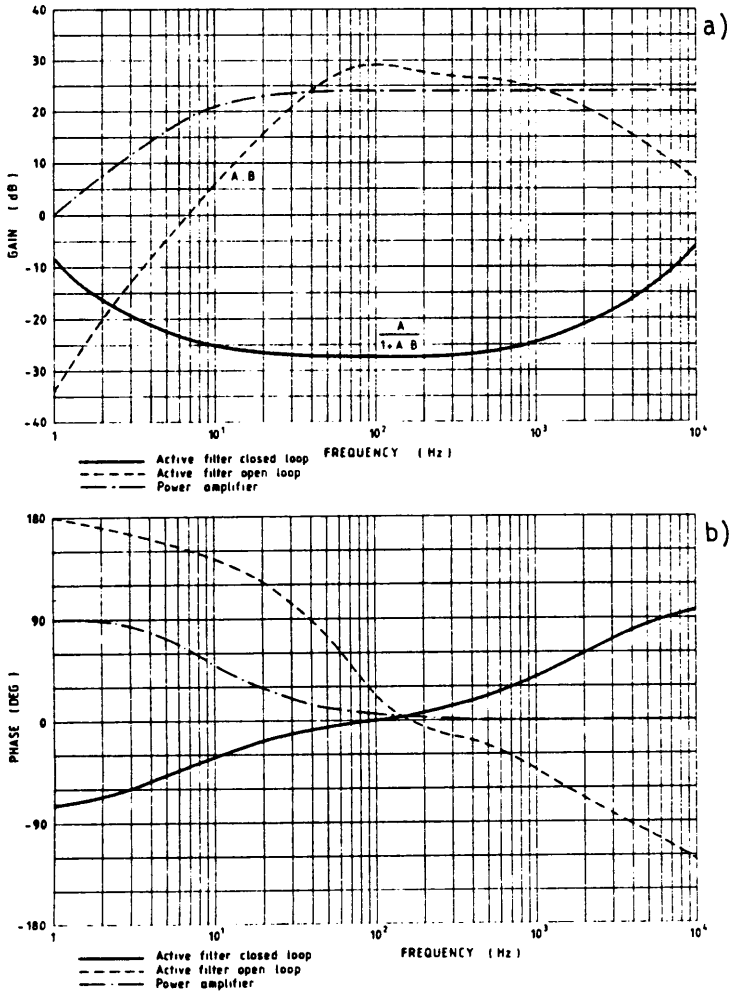

Fig. 9
Active filter loop transfer functions

Some relevant transfer functions of the active filter loop are shown in Fig. 9; they illustrate the characteristics and gain limits of the technical solution due to the influence of the passive filter, the load impedance, and the coupling choke.

In fact, owing to the impedance of the coupling choke, as well as to the capacitive coupling of the ripple voltage detection and power amplifier drive, the numerator of the active filter transfer function shown is of second order at low frequency and has to be corrected for current loop stability.

4.3.3 *Current-control loop*

The open-loop transfer function, without active filter, has a first-order integral characteristic at low frequency as usual for high-precision d.c. power supplies.

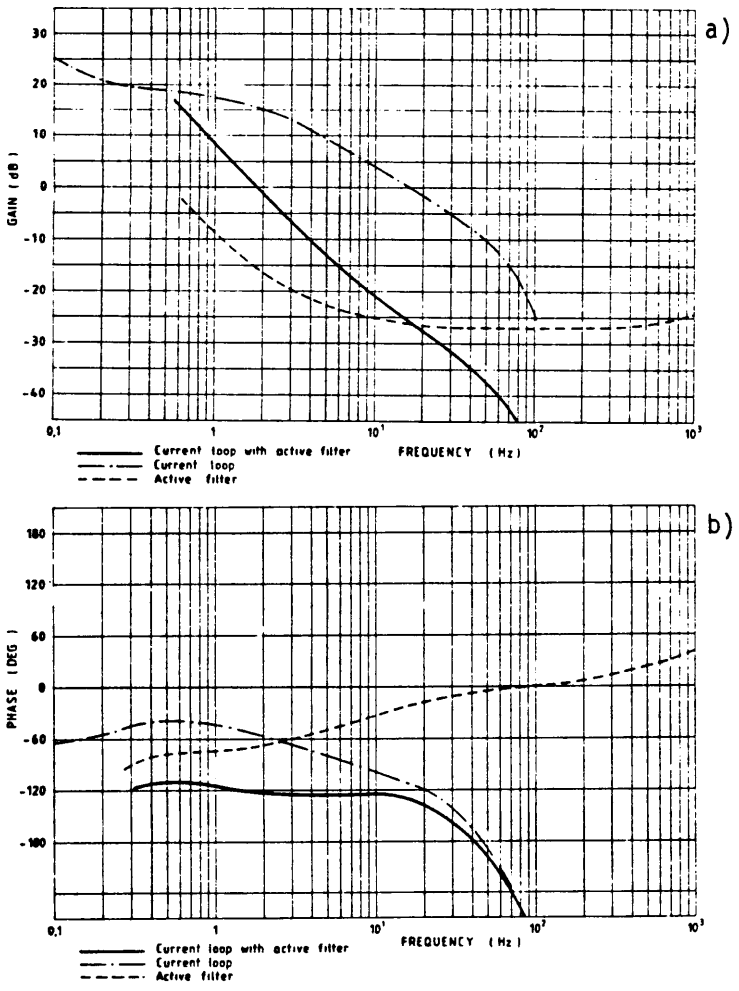

Fig. 10
Insertion of the active filter and current control transfer functions

To obtain a sufficient phase margin of the overall current-control transfer function, once the active filter is added, a suitable corrector has to be foreseen. The insertion of the active filter during operation and the resulting modification of the current open-loop transfer function is illustrated in Fig. 10. The magnet current is measured by a high-precision DCCT (HOLEC) of the type 3000 SH.

4.4 Electronics

The electronic printed-circuit boards (PCB's) are located in a (2 x 3U) Europe-crate.

The auxiliary power supplies, the gate-control set, the regulation and the active filter drive are in the upper part, while the microprocessor (μP 6809) assembly as well as the DAC, the ADC and interfacing cards connected to the G64 bus, are in the lower compartment. The lower front panel carries the touch panel and the (2x16 LED) character display for operating the power supply.

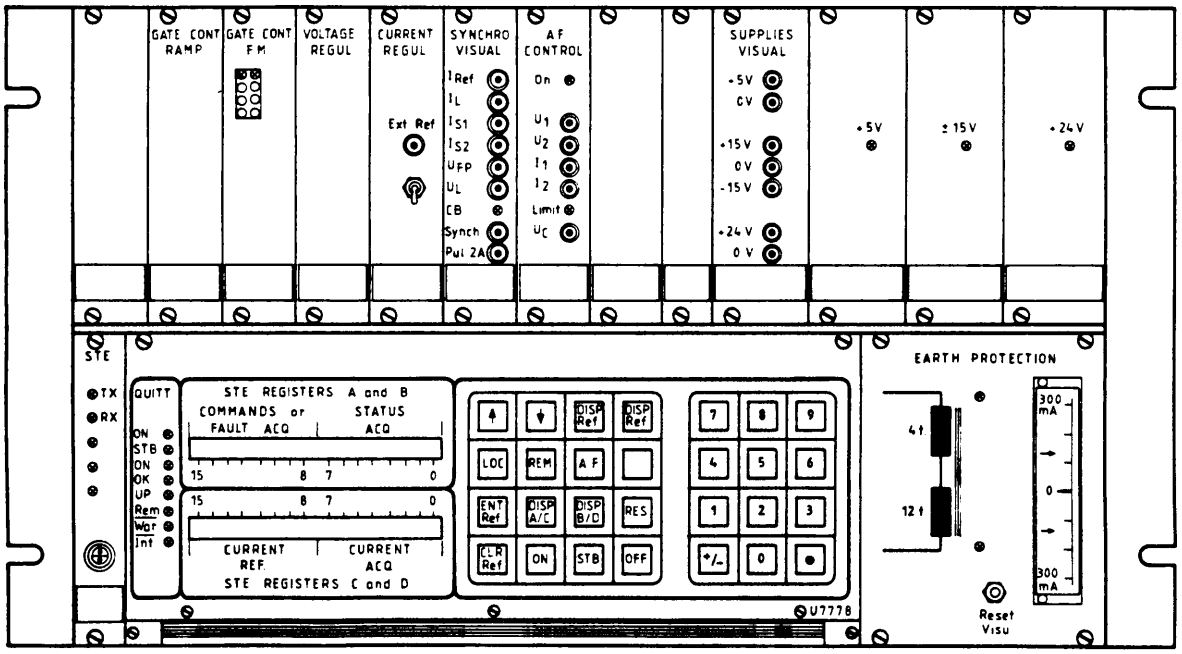

Fig. 11 Electronics crate and front-panel display

The interface function between power supply and central NORD-CAMAC computer system is implemented by a single transceiver card connected to the G64 bus. The electronics crate and the display are shown in Fig. 11.

The PS standard command and acquisition protocol is used:

- OFF (main circuit breaker out; gate control, regulation, and current reference inhibited);
- STAND BY (main circuit breaker in; electronics still inhibited);
- ON (electronics operating; output current according to reference);
- RESET (cancels the faults and restores the initial state; in the case of a persistent fault the remote reset actions within a given time interval are limited to three).

The magnet-current reference is given by a 14-bit DAC and the signal is treated by a rate and absolute-value limiting circuit.

The power supply can be operated under REMOTE control mode by computer through the Single Transceiver Europe (STE) interface board and under LOCAL control mode via the touch panel, and the LED display is managed by the μP unit.

4.5 Protections and interlocks

Besides the different protections and interlocks concerning the power components (such as primary transformer overcurrent; overtemperature of the magnetic components, of the thyristor rectifier, and of the active-filter amplifiers; fuses; water flow) the electronics is inhibited and the power disconnected in case of absence of any auxiliary voltage, load overcurrent, disturbance of the mains synchronization of the gate control, and external magnet faults.

The active filter amplifier has been protected with particular care by an auxiliary output current-limiting feed-

back circuit acting on its drive signal. Furthermore, during any transient, such as at switching on or when the magnet current reference is modified, the active filter is inhibited as long as the current error signal exceeds a certain level.

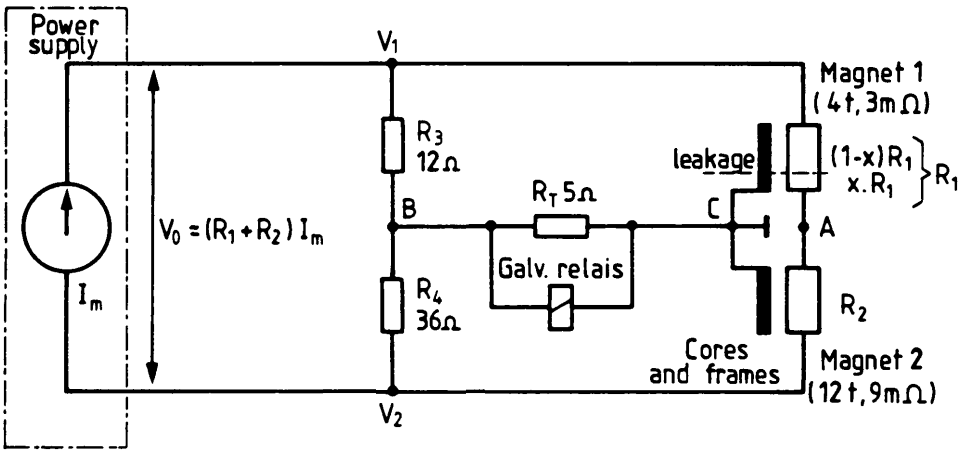

Fig. 12 Earth leakage current detector

Finally, the leakage current of the load to earth is detected by a circuit shown in Fig. 12. Taking into account that, as already mentioned, the load consists of two magnets with different resistance and the polarity of the power supply can be reversed, the floating midpoint (A) is normally kept at the electronics earth potential. The magnet core and support frame, insulated with respect to the winding, are connected to earth, while the power-supply divider midpoint is earthed through a resistor with a galvanometric relay in parallel. In the case of a leakage current to earth, owing to the degradation of the winding insulation, exceeding a preset level (between 15 mA and 300 mA), the power supply will be switched off and the magnet concerned will be detected.

$$\frac{R_1}{R_2} = \frac{R_3}{R_4} = \frac{1}{3} ,$$

$$U_B \text{ is } \simeq \frac{R_5}{R_5 + R_3 R_4/(R_3+R_4)} U_{B_0} = kU_{B_0} , \quad k = \frac{5}{14}$$

(U_{B_0} is the idle voltage at B),

$$U_B = - \text{ or } + I_m x R_1 k \text{ if leakage is on } R_1 \text{ or resp. on } R_2 .$$

4.6 Construction

The power section has been manufactured in industry (SCS-SALANO/Italy) according to a CERN technical specification [4]. The electronics has been developed and built at CERN for reasons of standardization and to simplify the exploitation of the equipment.

The power supply consists of three cubicles (see Fig. 2):

- A left-hand cubicle, which includes the a.c. and d.c. power connections, the a.c. switchgear, the transformer premagnetization circuit, the active-filter coupling choke, the DCCT, the polarity changer, and the electronics crate. One of the front doors is fitted with a synoptic diagram of the power circuit with a number of relevant measuring points.

- A cubicle with the four passive filter chokes, the passive filter capacitors and resistor assembly, the active filter drive, and its power assembly.

- A right-hand cubicle, including the two power transformers, the a.c. current-measuring transformers on the primary and secondary transformer sides, the four thyristor rectifiers, and the cooling-water circuit.

In defining the position of the power components and the cabling, particular attention has been paid to the operational aspects (safety, accessibility, and test facilities), to the separation of high- and low-power signals, and to the problem of good current sharing between the four parallel connected transformer secondaries, thyristor rectifiers, and filter chokes.

5. PERFORMANCE TEST RESULTS

The specified operational magnet current stability of 0,01%·In has been achieved by adapting the regulation to the given gate-control set and power-circuit layout and by improving the effectiveness of the active filter.

The problem of rejection of the external mains perturbations generated by other installations and transmitted through the a.c. distribution network has been investigated. In particular a series of tests concerning the effects on this d.c. power supply has been carried out when the PS Booster was pulsing at 800 MeV and 1 GeV.

These tests were done directly at the Booster. It can therefore be expected that the power supply will be less disturbed through the mains, once installed in its final place near the LPI machine. Some test results are shown in Fig. 13.

In addition, the losses of the different power-supply sections have been measured at nominal current, and the overall efficiency has been confirmed to be higher than the 85% design figure aimed at.

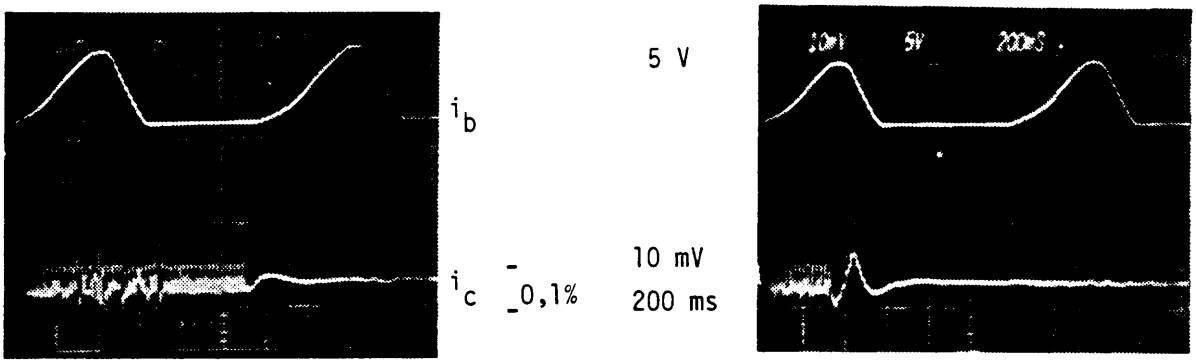

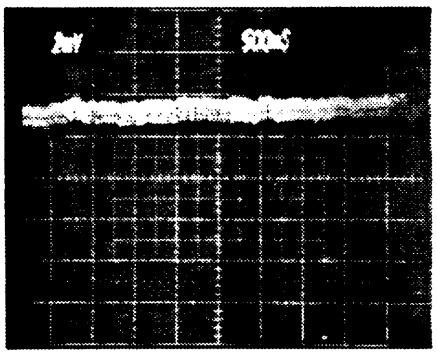

Fig. 13 Test results:
a) PS Booster at 1 GeV and 800 MeV: magnet current when the active filter is put into operation.
b) PS Booster at 1 GeV: magnet current stability.

6. CONCLUSIONS

It has been shown that high conversion efficiency can be achieved in high-current low-voltage d.c. power supplies, by using separate transformers, 3-way thyristor rectifiers, and separate passive filter chokes without interphase reactors.

A simple active filter concept has been developed for this type of power supply, which is particularly suitable for replacing series transistor regulators in existing equipment for the sake of energy saving.

The technical specifications have been comfortably satisfied despite the intrinsic limitation imposed by the gate control set used here for practical reason of project time schedule and of standardization. A further factor of more than two in current stability performance is potentially achievable.

The μP unit on the G64 bus, integrated in the electronics crate, is an interesting example of the evolution of the man-equipment interface in the case of power supplies in the high-energy physics accelerator environment.

ACKNOWLEDGEMENTS

We would like to express our thanks to J. Madsen, LPI project leader, and to L. Coull, PO group leader, who entrusted this work to us.

We would also like to thank the colleagues who contributed to the programming and testing of the μP unit as well as to the installation and putting into operation of the power supplies.

Finally, we would like to mention the excellent collaboration we had with industry in the course of this project, and the enthusiasm we met there in building and thoroughly factory-testing the power supplies.

This report has been typed and edited by the Scientific Typing Service at CERN.

REFERENCES

1. The LEP Injector Study Group, The chain of LEP injectors, CERN-LEP/TH/83-15 Rev., presented at the Particle Accelerator Conference, Santa Fe, New Mexico, 1983.

2. The LEP Injector Study Group, LEP design report, Vol. 1, CERN-LEP/TH/83-29 (1983).

3. B. Boileau, P. Pearce and R. Valbuena, The Injection and Ejection Septum Magnets of the LEP-EPA, CERN/PS/BT/85-50 (1985).

4. Spécification technique des alimentations à courant continu 3 kA, 40 V pour les aimants à septum de l'EPA, CERN-PS/LPI/MM/SPEC 84-2 (1984).

APPENDIX A

Inrush current limiting circuit

Let us consider the simplified equivalent circuit of the power transformer (see Fig. A1), drawing an idle magnetizing current i, corresponding to n % of nominal current and assumed quasi-sinusoidal, when the nominal voltage U_n is applied.

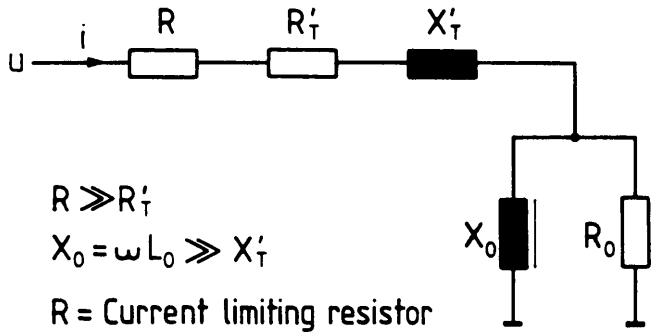

Fig. A1 Equivalent circuit of transformer

The initial shape of the magnetizing current is principally determined by the point of the voltage wave at which switching-in occurs, but it is also partly dependent on the magnitude and polarity of the residual magnetic induction left in the core. The worst case is when switching in occurs at zero-voltage crossing with maximum residual magnetic flux Φ_r. The maximum flux achieved in that core will be $\Phi_M = \Phi_r + \int(u-Ri)dt$.

Assuming the applied voltage to be

$$u = \sqrt{2}\, U_n \sin(\omega t+\gamma) \simeq Ri + L_0\, di/dt ,$$

and assuming L_0 to be linear, one obtains

$$i = \frac{\sqrt{2}\, U_n}{Z} \left[\sin(\omega t+\gamma-\varphi) - e^{-(t/T_0)} \sin(\gamma-\varphi)\right] ,$$

where

$$T_0 = \frac{L_0}{R} ,$$

$$Z = (R^2+\omega^2 L_0^2)^{1/2} = \omega L_0 \left[1 + \frac{1}{\omega^2 T_0^2}\right]^{1/2} ,$$

$$\varphi = \text{arctg}(\omega T_0) .$$

In the worst case, for $\gamma = 0$, one can write for the flux in the core (Φ_r is assumed to be negligible)

$$\Phi = L_0 i = \frac{\sqrt{2}\, U_n}{\omega} \sin\varphi \left[\sin(\omega t-\varphi) + e^{-(t/T_0)} \sin\varphi\right] .$$

Taking as parameter $\text{tg}\,\varphi = \omega T_0 \simeq (100\, U_L^2/nP)(1/R)$, U_L being the line-to-line voltage and P the nominal transformer rating, one draws the function $(L_0 i/\int_0^{T/4} u\, dt)$ with respect to ωt and derives the diagram of the maximum flux values achieved at switch in as a function of $\text{tg}\,\varphi = \omega T_0$ (Fig. A2).

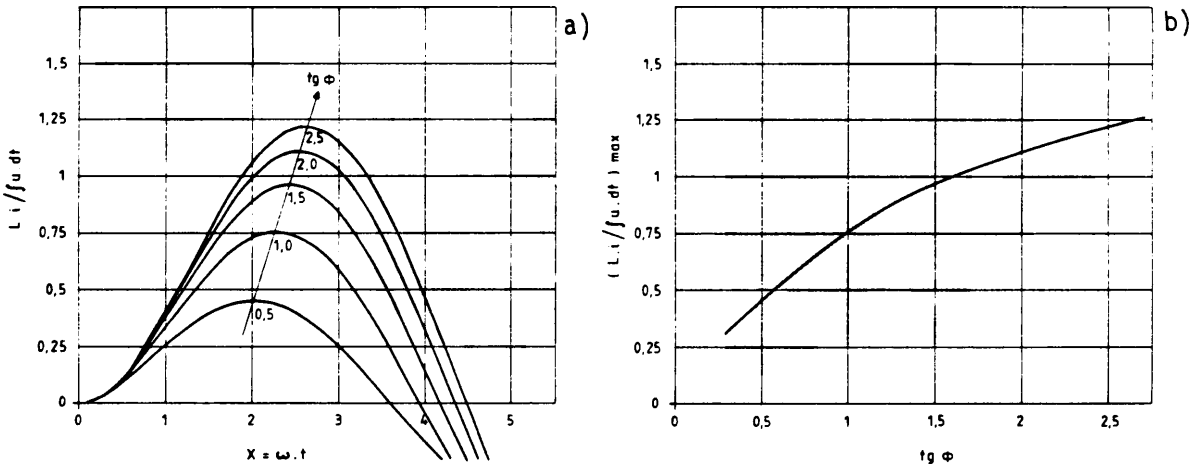

Fig. A2 a) Flux evolution with time after switching in.
b) Diagram of maximum flux amplitudes.

The value of the inrush current-limiting resistor R and its theoretical power ratings, in the case of a permanent magnetizing current and neglecting the fact that, in practice, the resistor is short-circuited after a few seconds, are given by the expressions

$$R = \left[\frac{100\ U_L^2}{nP}\right] \frac{1}{tg\ \varphi}\ ,$$

$$P_R = \left[\frac{U_L^2}{3R}\right] \frac{1}{(1+tg^2\varphi)} = \left[\frac{nP}{300}\right] \left[\frac{tg\ \varphi}{1+tg^2\varphi}\right]\ .$$

A diagram of (R,P_R) for tg φ = 1.5 is given in Fig. A3. Entering the value of $U_L^2/nP(kVA)$ yields R and P_R.

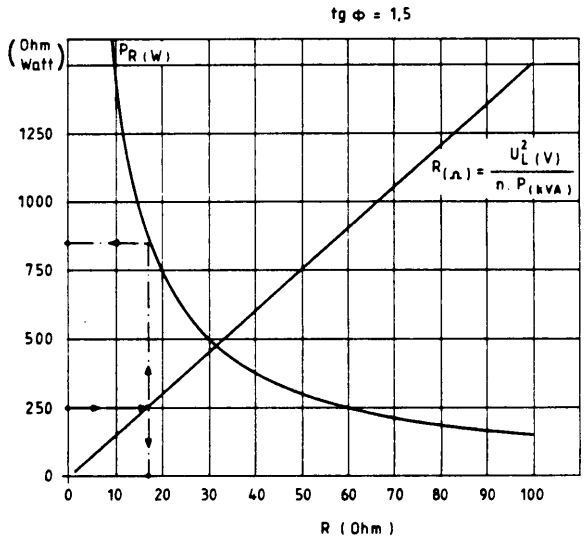

Fig. A3
Determination of the
resistor value and power ratings

APPENDIX B

Extended delta/star 3-phase transformer

1. Transformer design

The vector diagram for the two mains connections RST and RTS is given in Fig. B1. The following relationships can be derived for a general phase shift $0 < \varphi < 30°$

$$\varepsilon = 1 + \frac{n_a}{n_b} = \frac{\sin(30+\varphi)}{\sin(30-\varphi)} = \frac{1 + \sqrt{3}\,\mathrm{tg}\,\varphi}{1 - \sqrt{3}\,\mathrm{tg}\,\varphi} ,$$

$$\frac{n_c}{n_b} = (\varepsilon^2+\varepsilon+1)^{1/2} ,$$

$$\frac{n_c}{n_a} = \frac{(\varepsilon^2+\varepsilon+1)^{1/2}}{(\varepsilon-1)} ,$$

$$n_c = n_b[\varepsilon \cos(30-\varphi) + \cos(30+\varphi)] = n_b\,\eta .$$

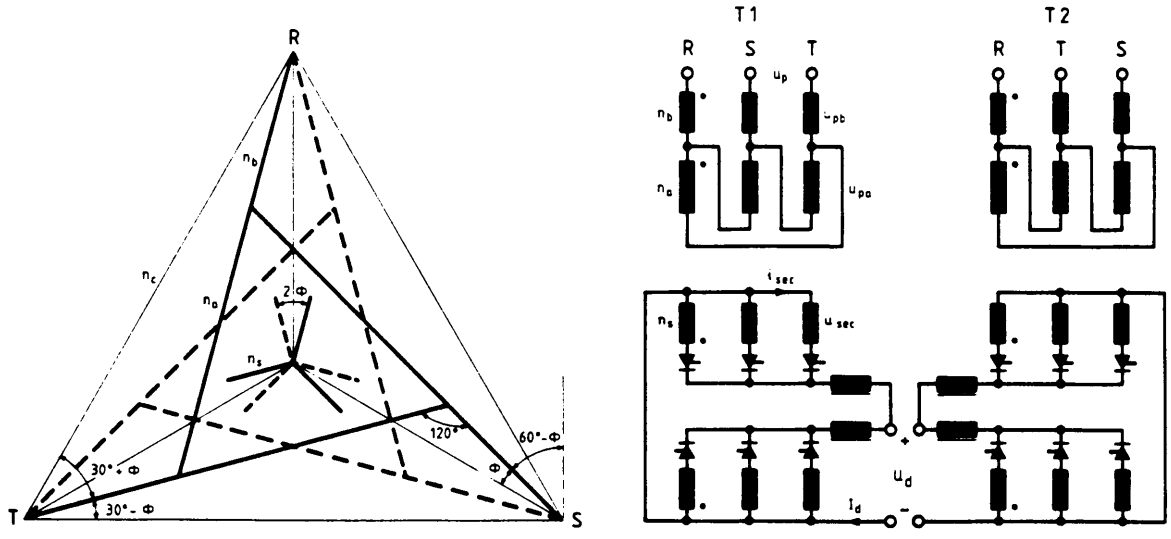

Fig. B1 Transformer vector diagram and connection

The coefficients ε and η are drawn in Fig. B2 as a function of the phase shift φ.

Assuming a transformer, fed by the primary voltage U_p having one secondary with phase voltage U_{sec} and phase shift φ, one

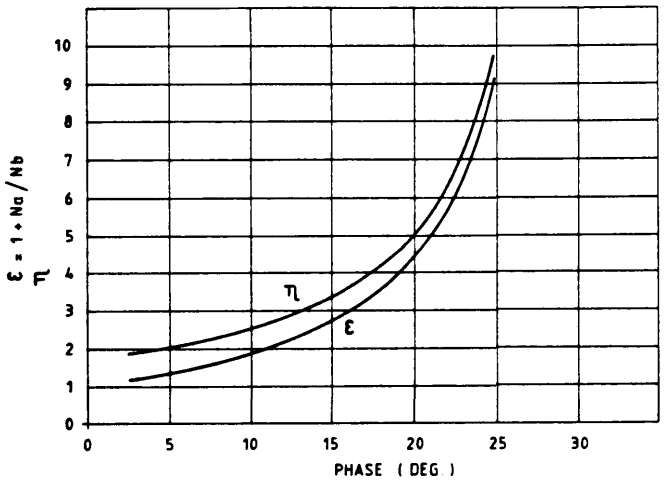

Fig. B2
Coefficients ε and η

indicates by U_p/n_c the volts per turn parameter and by $n_s = (U_{sec}/U_p)n_c$ the theoretical secondary number of turns.

Choosing either n_c or n_s one obtains n_a and n_b as well as the voltage across the two sections of primary windings

$$U_{pa} = U_p \frac{n_a}{n_c} \quad , \quad U_{pb} = U_p \frac{n_b}{n_c} \quad .$$

In general, the ampere-turn compensation on each column b imposes

$$i_{pa} = \frac{n_s}{n_b} \frac{[i_R''\varepsilon^2 + i_S''\varepsilon + i_T'']}{(\varepsilon^3-1)}$$

and

$$i_{pb} = \frac{n_s}{n_b} \left[\frac{i_R''(\varepsilon^2-1) + i_S''(\varepsilon-\varepsilon^2) + i_T''(1-\varepsilon)}{(\varepsilon^3-1)} \right] ,$$

where i_R'', i_S'', i_T'' are the instant secondary phase currents. By projecting i_{pa} and i_{pb} on the real and imaginary axes one obtains the components of the effective currents I_{pa} and I_{pb}, and by the square roots of the sum of the squares of the components one gets

$$I_{pa} = \frac{n_s}{n_b} I_{sec} K_{pa} \quad , \qquad I_{pb} = \frac{n_s}{n_b} I_{sec} K_{pb} \quad .$$

The coefficients K_{pa} and K_{pb} are drawn in Fig. B3 as a function of the phase shift φ.

In the particular case of $\varphi = 15°$ one obtains

$$I_{pa} = \frac{n_s}{n_b}\frac{1}{\eta} I_{sec} = \frac{n_s}{n_c} I_{sec} ,$$

$$I_{pb} = \frac{n_s}{n_c} I_{sec} \sqrt{3} .$$

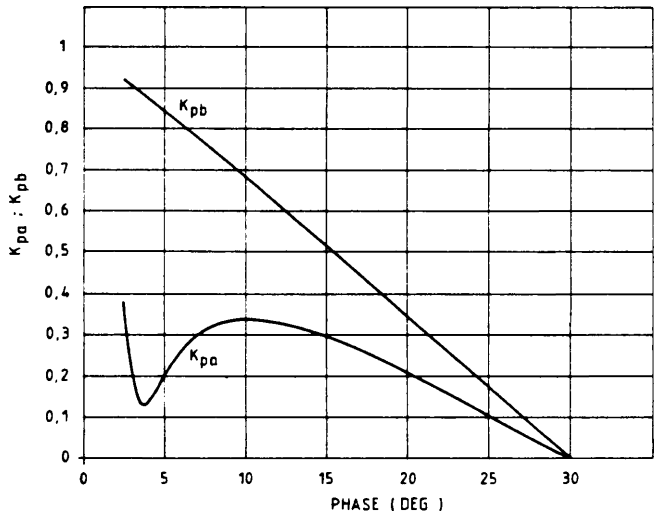

Fig. B3 Coefficients K_{pa} and K_{pb}

The following general relationships give the power ratings of the transformer primary and secondary windings and the design ratings P_T.

$$P_p = 3(U_{pb}I_{pb} + U_{pa}I_{pa}) = 3\ M\ U_{sec}\ I_{sec}$$

$$P_{sec} = 3\ U_{sec}\ I_{sec} = \begin{cases} 1.05\ P_d & \text{Graez rectifier} \\ 1.51\ P_d & \text{3-way rectifier} \\ 1.48\ P_d & \text{3-way with interphase reactor or paralleling via separate filter chokes} \end{cases}$$

$$P_T = \frac{(P_p + P_{sec})}{2} = \left[\frac{M+1}{2}\right] P_{sec} = M_b P_d .$$

The coefficients M and M_b (for the case of the 3-way rectifier and interphase reactors) are drawn in Fig. B4 as a function of the phase shift φ.

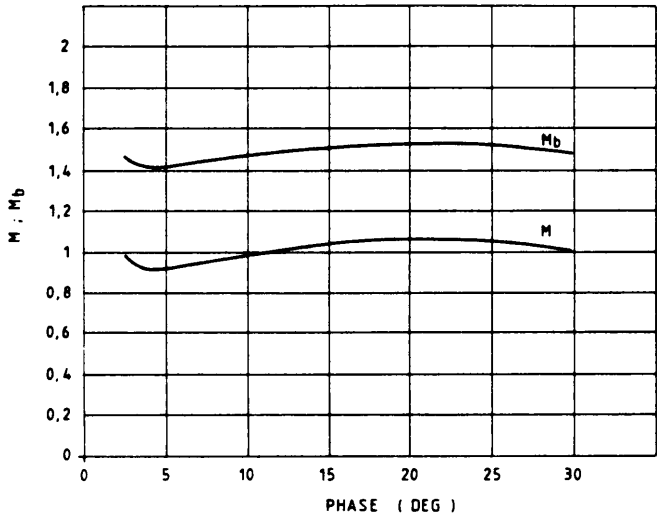

Fig. B4 Coefficients M and M_b

2. Ampere-turn compensation

Considering in Fig. B5 the rectifier transformer with two star secondaries feeding two 3-way rectifiers one obtains the instant primary currents:

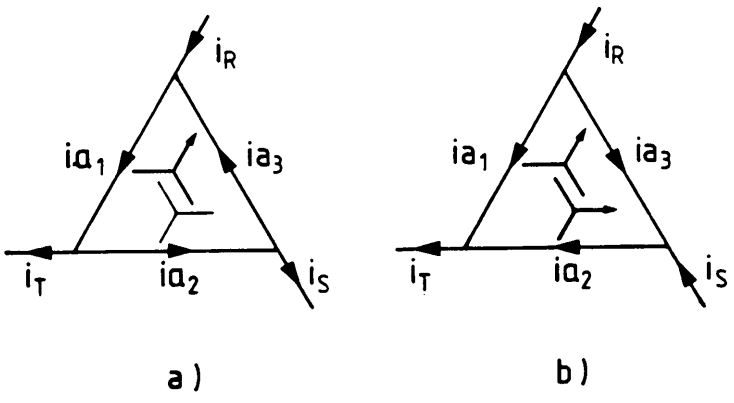

Fig. B5 Diagram of primary currents

a) When one secondary phase conducts

$$\begin{cases} i_{a1} = \dfrac{i_{sec} n_s}{n_b} \left[\dfrac{\varepsilon^2}{\varepsilon^3 - 1}\right] \\ i_{a2} = \dfrac{i_{sec} n_s}{n_b} \left[\dfrac{\varepsilon}{\varepsilon^3 - 1}\right] \\ i_{a3} = \dfrac{i_{sec} n_s}{n_b} \left[\dfrac{1}{\varepsilon^3 - 1}\right] \end{cases} \qquad \begin{cases} i_R = \dfrac{i_{sec} n_s}{n_b} \left[\dfrac{\varepsilon + 1}{\varepsilon^2 + \varepsilon + 1}\right] \\ i_S = \dfrac{i_{sec} n_s}{n_b} \left[\dfrac{1}{\varepsilon^2 + \varepsilon + 1}\right] \\ i_T = \dfrac{i_{sec} n_s}{n_b} \left[\dfrac{\varepsilon}{\varepsilon^2 + \varepsilon + 1}\right] \end{cases}$$

b) When two secondary phases conduct

$$\begin{cases} i_{a1} = \dfrac{i_{sec} n_s}{n_b} \left[\dfrac{1 + \varepsilon}{\varepsilon^2 + \varepsilon + 1}\right] \\ i_{a2} = \dfrac{i_{sec} n_s}{n_b} \left[\dfrac{\varepsilon}{\varepsilon^2 + \varepsilon + 1}\right] \\ i_{a3} = \dfrac{i_{sec} n_s}{n_b} \left[\dfrac{1}{\varepsilon^2 + \varepsilon + 1}\right] \end{cases} \qquad \begin{cases} i_R = \dfrac{i_{sec} n_s}{n_b} \left[\dfrac{\varepsilon + 2}{\varepsilon^2 + \varepsilon + 1}\right] \\ i_S = \dfrac{i_{sec} n_s}{n_b} \left[\dfrac{\varepsilon - 1}{\varepsilon^2 + \varepsilon + 1}\right] \\ i_T = \dfrac{i_{sec} n_s}{n_b} \left[\dfrac{2\varepsilon + 1}{\varepsilon^2 + \varepsilon + 1}\right] \end{cases}$$

In this case one can imagine a virtual circulation current $i_c = (i_{sec} n_s / n_b)[1/(\varepsilon^2 + \varepsilon + 1)]$ flowing inside the triangle and providing for ampere-turn compensation.

To facilitate the computation the above coefficients have been collected in Table B1 for $\varphi = 15°$ and $\varepsilon = 2.732$.

Table B1

Coefficients for $\varphi = 15°$ and $\varepsilon = 2.732$

$\varepsilon = 2.732$ $(\varepsilon^3-1) = (\varepsilon-1)(\varepsilon^2+\varepsilon+1)$	$\varepsilon^2+\varepsilon+1 = 11.196$	$\frac{1}{\varepsilon^2+\varepsilon+1} = 0.089$
$\frac{\varepsilon}{\varepsilon^2+\varepsilon+1} = 0.244$	$\frac{\varepsilon+1}{\varepsilon^2+\varepsilon+1} = 0.333$	$\frac{2\varepsilon+1}{\varepsilon^2+\varepsilon+1} = 0.577$
$\frac{\varepsilon+2}{\varepsilon^2+\varepsilon+1} = 0.422$	$\frac{\varepsilon-1}{\varepsilon^2+\varepsilon+1} = 0.155$	$\frac{n_s}{n_b} = \frac{U_{sec}}{U_p}\eta$

3. Choice of n_a and n_b and resulting phase-angle error $\left(\frac{\varphi-\varphi_0}{\varphi_0}\right)\cdot 100$ for $\varphi_0 = 15°$

From the relationship $\varphi = \text{arctg}\left[\frac{\varepsilon-1}{\sqrt{3(\varepsilon+1)}}\right]$ for different values of n_a and n_b, the error in phase-shift angle φ has been calculated in the case of $\varphi_0 = 15°$ and $U_p = 380$ V, and collected in Table B2.

Table B2

Selection of primary turns and phase-shift angle error
($\varphi_0 = 15°$ and $U_p = 380$ V)

n_a	n_b	n_a/n_b	n_c	φ (degree)	Phase angle error (%)	U_{pa} (V)	U_{pb} (V)
19	11	1.7272	36.755	14.978	-0.142	196.43	113.72
26	15	1.7333	50.209	15.005	0.037	196.77	113.52
45	26	1.7307	86.965	14.994	-0.038	196.62	113.60
64	37	1.7297	123.721	14.989	-0.069	196.57	113.64
71	41	1.7317	137.175	14.998	-0.011	196.68	113.57
83	48	1.7291	160.477	14.987	-0.086	196.53	113.66
85	49	1.7346	164.082	15.011	0.078	196.85	113.47
88	51	1.7254	170.326	14.970	-0.195	196.32	113.78
97	56	1.7321	187.384	15.000	0.002	196.70	113.56

APPENDIX C

Harmonic content of load voltage after the LCR passive filter

To evaluate the residual harmonics content after the passive filter, which the active filter has to cancel, the following procedure has been used. The four thyristor rectifiers are considered as a.c. voltage sources feeding the passive filter chokes. In the general case of n sources U_i, shown in Fig. C1, feeding n chokes X_i, one can derive the relationship

$$u = \frac{\sum_{i=1}^{n} \left(u_i \prod_{j \neq i}^{n} X_j \right)}{\sum_{i=1}^{n} \prod_{j \neq i}^{n} X_j} \quad , \qquad X = \frac{\prod_{i}^{n} X_i}{\sum_{i=1}^{n} \left(\prod_{j \neq i}^{n} X_j \right)} \quad , \qquad u_r = \frac{u}{1 + \frac{X}{X_c}} \; .$$

In the case where n = 4 and all filter chokes are equal ($X_i = X_0$) the relationships become

$$u = \frac{\sum_{i=1}^{4} u_i}{4} \quad , \qquad X = \frac{X_0}{4} \quad , \qquad u_r = \frac{\sum_{i=1}^{4} u_i}{4 + (X/X_c)} \; .$$

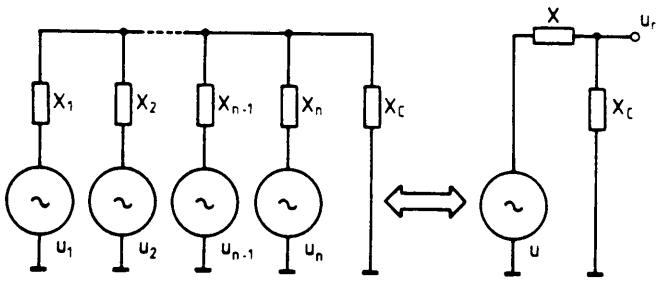

Fig. C1
Equivalent circuit
for n rectifiers and chokes

In first approximation, the effect of the passive filter can be reduced to

$$u_r = \frac{\sum_{i=1}^{4} u_i}{4 + (f/f_0)^2}$$

where f_0 is the equivalent corner frequency of the filter, and $\sum_{i=1}^{4} u_i$ is the Fourier series of the voltage waveforms in front of the filter

$$\sum_{i=1}^{4} u_i = \sum_{i=1}^{4} \left[\frac{a_0 i}{2} + \left(\sum_j a_{ij} \cos \omega t + \sum_j b_{ij} \sin \omega t \right) \right] .$$

On the basis of the waveform diagram of Fig. C2 the Fourier coefficients of the rectified voltage after the passive filter have been calculated, taking into account the a.c. phase-voltage

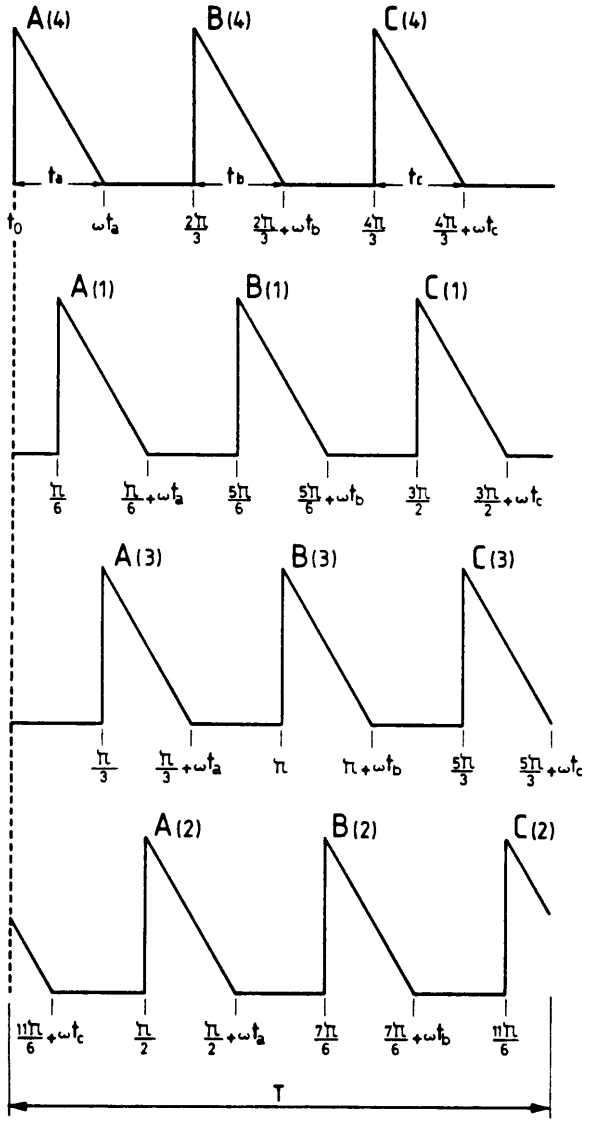

Fig. C2 Waveforms for the Fourier analysis of the rectified voltage

$$U_i(t) \simeq A\left[1 - \left(\frac{t-t_0}{t_a}\right)\right] + B\left[1 - \left(\frac{t-t_1}{t_b}\right)\right] + C\left[1 - \left(\frac{t-t_2}{t_c}\right)\right]$$

dissymmetries due to the actual magnetic components (derived from the results of factory tests) as shown in Table C1.

Table C1

Amplitude of harmonics in the d.c. voltage after the passive filter

Order of harmonic f/50	Computed amplitude (V)
1	0.012
2	0.067
3	0.03
4	0.03
5	0.005
6	0.03
7	0.003
8	0.011
9	0.008
10	0.016
11	--
12	2.12
24	1.06
36	0.71

The load voltage at nominal current is ~ 38 V and the specified 0.01% current ripple amplitude corresponds to 0.272 A or to 0.031(f/50) V for any harmonic.

The computation shows that subharmonics must also be reduced by the active filter. The computation can be repeated for any dissymmetry of the rectified voltage.

APPENDIX D

Active ripple filter

The equivalent circuit, shown in Fig. D1(a), is used to analyse the mode of operation of the active filter and to derive the basic relationships for its design.

The iron losses of the coupling choke have been neglected, owing to the small induction variations, as well as the stray inductance $L_\sigma << m^2 L_2 (m = N_1/N_2)$, measured when the secondary is short-circuited.

For given choke ratings and dimensions the ratio $m^2 L_2/R_1$ does not vary much if one changes the number of primary turns. This ratio defines the low-frequency characteristic of the choke.

The active filter output voltage U_{AF} is supposed to be derived from the load voltage U_L via a general transfer function K(s), which includes the measuring, drive, and power-stage circuits.

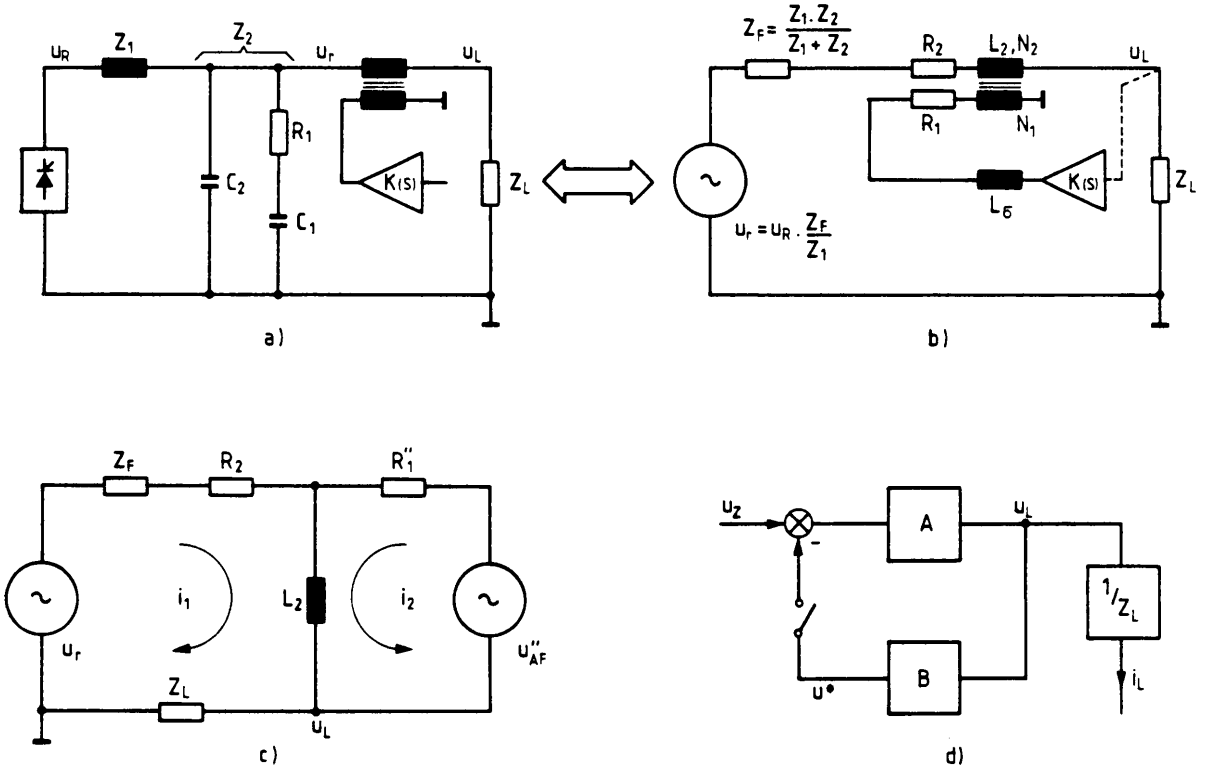

Fig. D1 Equivalent active filter circuits

The impedance of the secondary winding of the active filter choke is $(R_2 + sL_2)$. Relating the circuit parameters to the secondary

winding, as shown in Fig. D1(b), one can derive the following relationships:

$$i_1 = \frac{U_r(R_1''+sL_2) - U_{AF}''sL_2}{(R_1''+sL_2)(R_2+Z_L+Z_F) + R_1''sL_2} ,$$

$$i_{AF}'' = \frac{U_{AF}''\,[(R_2+sL_2) + (Z_F+Z_L)] - U_r sL_2}{(R_1''+sL_2)(R_2+Z_F+Z_L) + R_1''sL_2} ,$$

$$\frac{U_L}{U_r} = \frac{(R_1''+sL_2)Z_L}{[(R_1''+sL_2)(R_2+Z_F+Z_L) + R_1''sL_2] + sL_2Z_LK(s)} ,$$

where Z_L is the load impedance, $Z_F = Z_1Z_2/(Z_1+Z_2)$ is the passive filter impedance, and the active filter voltage referred to the secondary U_{AF}'' is equal to $[K(s)U_L]$ with $K(s) = K'(s)/m$. To translate these expressions into terms of transfer functions one refers to Fig. D1(c), where

$$\frac{U^*}{U_L} = B = K(s)\left(\frac{sL_2}{R_1'' + sL_2}\right)$$

and

$$A = \frac{Z_L}{(R_2+Z_L+Z_F) + (R_1''sL_2)/(R_1''+sL_2)} .$$

The overall open-loop transfer function is given by

$$\frac{U^*}{U_r} = A\,B = K(s)\frac{sL_2Z_L}{R_1''sL_2 + (R_2+Z_L+Z_F)(R_1''+sL_2)}$$

and the closed-loop transfer function is U_L/U_r, as already given above.

The term $[sL_2/(R_1''+L_2s)]$, due to the unavoidable resistance of the primary active filter-choke winding, introduces a break point typically in the 10 Hz region (see Fig. 9).

To illustrate the effect of the load and filter impedance the amplitude and phase of Z_L, Z_F, and $Z_L + Z_F$ have been drawn in Fig. D2. In the present case $R_2 << R_1 << R_L$ and $L_2 \simeq 7L_L$, while m = 17.

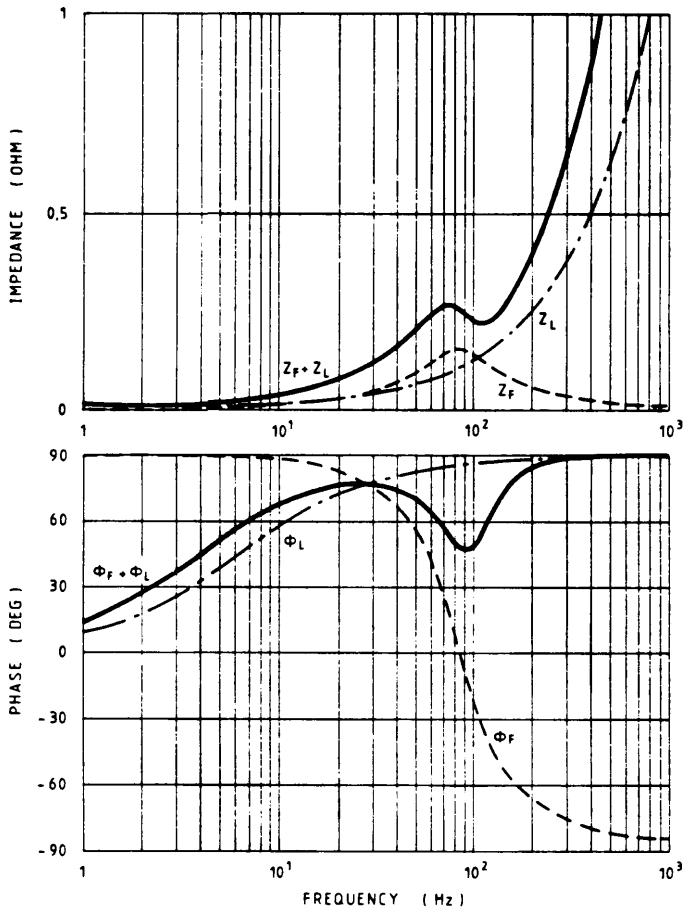

Fig. D2 Amplitude and phase of load and filter impedances

For a more general discussion of the active-filter design let us rewrite some relationships under the assumption that R_1'' and R_2 can be neglected

$$U_{AF} = m\,K(s)\frac{U_r}{1 + K(s) + (Z_F/Z_L)}\,,$$

$$i_{AF} = \frac{1}{m}\frac{U_r}{(Z_F+Z_L)}\left[\frac{K(s)\cdot(Z_F+Z_L)}{sL_2[1 + K(s) + Z_F/Z_L]} - 1\right] \simeq \frac{U_r\,K(s)}{m\,sL_2[1+K(s)+Z_F/Z_L]}$$

if $Z_L >> sL_2$.

The expression of the active filter ratings becomes

$$P_{AF} = i_{AF}U_{AF} = \frac{U_r^2}{sL_2}\left[\frac{K(s)}{1+K(s)+Z_F/Z_L}\right]^2 .$$

For given U_R and load impedance Z_L the design will depend on the choice of Z_1 and Z_F/Z_1 [$U_r = U_R(Z_F/Z_1)$], as well as on R_2, L_2, and on the ratio of turns m.

Stability criteria, depending on the correctors in the active filter loop, will determine the appropriate value of K(s).

In the case of $(Z_L+Z_F) >> sL_2$ and neglecting R_1'' and R_2, one obtains

$$\frac{U_L}{U_r} = \frac{1}{K(s) + 1 + (Z_F/Z_L)} \qquad \text{and} \qquad \begin{cases} A \simeq \dfrac{1}{1 + (Z_F/Z_L)} \\ B \simeq K(s) \end{cases}$$

$$A\,B = \frac{K(s)}{1 + (Z_F/Z_L)} .$$

The above relationships indicate the influence of the different parameters on the active filter loop stability and performance. The low frequency response of the active filter loop is of great importance in practice.